IJAMB
INTERNATIONAL JOURNAL OF ADVANCES IN MEDICAL BIOTECHNOLOGY

Effect of Nb_2O_5 on the aging and cytotoxicity of ZrO_2-Y_2O_3 based biomaterial

J. C. Paiva[1]*; P. Leo[2]; C. Fredericci[2]; L. A. Bueno[1]
[1]Federal University of ABC (UFABC)
[2]Institute of Technological Research (IPT)
*Corresponding author: e-mail address: julio.carvalhopaiva@gmail.com
Received: August 2025; Accepted: December 2025

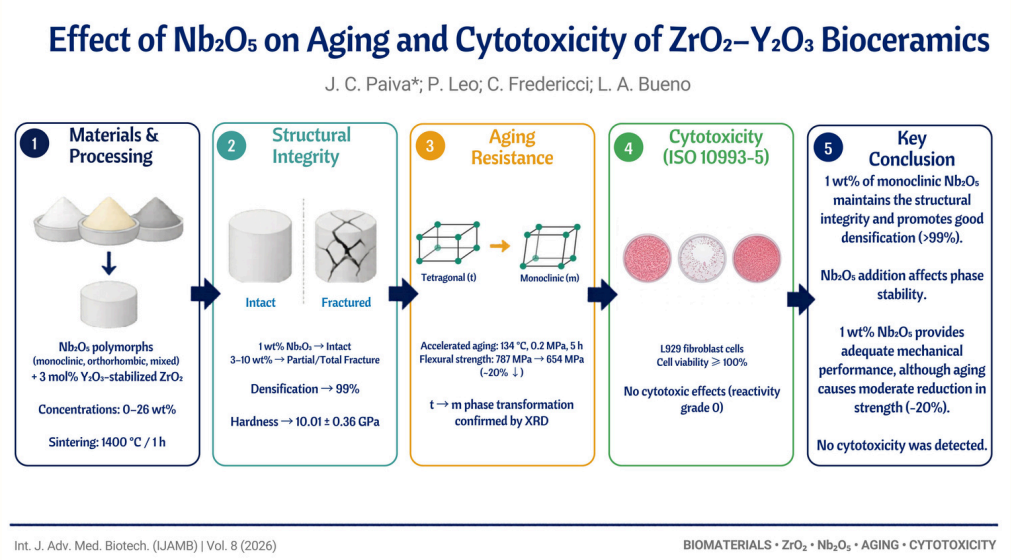

Abstract: This study investigates the influence of different polymorphs and concentrations of niobium pentoxide (Nb_2O_5) on the aging resistance and cytotoxicity of Y_2O_3-stabilized zirconia (ZrO_2) bioceramics. The goal was to evaluate the structural, mechanical, and biological responses of ZrO_2–Y_2O_3–Nb_2O_5 systems, addressing concerns related to low-temperature degradation (LTD) in biomedical applications. Different polymorphs of Nb_2O_5 (monoclinic, orthorhombic, and mixtures) were incorporated at various concentrations (1–26 wt%) into 3 mol% Y_2O_3-stabilized ZrO_2 and processed through controlled sintering cycles. Phase compositions were characterized by X-ray diffraction and Raman spectroscopy. Mechanical and microstructural properties were evaluated through density measurements, Vickers microhardness, flexural strength testing, and SEM imaging. Accelerated aging tests simulated long-term in vivo conditions, and cytotoxicity was assessed via in vitro assays using L929 fibroblast cells in accordance with ISO 10993-5. Results demonstrated that the addition of 1 wt% monoclinic Nb_2O_5 maintained structural integrity, mechanical strength, and biocompatibility, while higher concentrations led to cracking and tetragonal phase destabilization. Aging led to a moderate reduction in mechanical strength, and no cytotoxic effects were observed. The findings suggest that low-level monoclinic Nb_2O_5 doping may enhance ZrO_2's viability for biomedical use.
Keywords: Biomaterials, ZrO_2, Nb_2O_5, Aging, Cytotoxicity

https://doi.org/10.52466/ijamb.v8i1.159

Vol. 8 (2026) e-ISSN: 2595-3931

Introduction

It is well known that zirconia has intrinsic physical and chemical properties such as high hardness, wear resistance, low friction coefficient, and chemical inertness, which make it a material of interest for biomaterial applications [1, 2, 3]. It was only after the 1970s that there was an increase in zirconia applicability due to the understanding of the stabilization mechanism of the monoclinic (m) to tetragonal (t) ZrO_2 phase transformation and its toughening [4]. Studies have revealed that Y_2O_3, CeO_2, CaO, and MgO doping is essential to retain the tetragonal or cubic phase of ZrO_2, avoiding an increase in sample volume of approximately 3 to 4%. The most commonly used in medicine and dentistry is 2-3.5 mol% Y_2O_3-doped ZrO_2 (Y-TZP) [5]. The use of partially toughened zirconia as a biomaterial, especially as a femoral head, was successful from 1986 until about 2001. In 2001, reports indicated that 400 femoral implants failed within a short period, leading to concerns about the reliability of zirconia as an implant biomaterial [6-7]. The failure was attributed to accelerated aging of the metastable zirconia in an aqueous environment [3-8], known as low temperature degradation (LTD) which results in spontaneous and progressive t-m transformation thus compromising its mechanical properties. Alternatives have been proposed for improving the LTD resistance in the ZrO_2-Y_2O_3 system by adding secondary phase to it such as Al_2O_3, Nb_2O_5, Ta_2O_5, Gd_2O_3, Sm_2O_3, Yb_2O_3, and Sc_2O_3 [9-11]. Regarding to Nb_2O_5, most of the published papers do not mention the polymorph used for the preparation of ZrO_2-Y_2O_3 ceramic [12-17]. Like zirconium oxide, niobium oxide undergoes a series of phase transformations depending on temperature. Although it is reported that Nb_2O_5 exhibits different polymorphic crystalline phases such as orthorhombic, tetragonal, pseudohexagonal, and monoclinic as well as one amorphous phase ($Nb_2O_5.nH_2O$), the most common are low-temperature orthorhombic (< 1000 °C) and high-temperature monoclinic (≥ 1000 °C) forms [18-21]. When it comes to the use of ZrO_2-Y_2O_3 ceramics as biomaterials, knowledge of cytotoxicity is as important as the aging process. Thus, this work aims to analyze the impact of Nb_2O_5 polymorphism and content on the aging behavior and cytotoxicity of the ZrO_2-Y_2O_3-Nb_2O_5 system.

Material and Method

Nb_2O_5 CBMM was used as received (a mixture of monoclinic and orthorhombic), Nb_2O_5 CBMM treated at 1000 °C/3 h (monoclinic), Nb_2O_5 Merck (orthorhombic), and TZ-3YSB-E Tosoh (3% Y_2O_3). Initially, the sintering of the mentioned niobium oxides was studied to verify whether the polymorphic transformation would cause any degradation of the specimens, since, like zirconia, phase transformations in niobium oxide lead to volumetric variations. Specimens were prepared by pressing at 400 MPa in 11 mm diameter molds and sintered at 1400 °C for 1 h.

Next, the effect of the type of niobium oxide on the sintering of TZ-3YSB-E was studied. In this case, mixtures were prepared with compositions presented in Table 1. The mixing process was carried out dry. The oxides were sieved using a 320-mesh sieve (TLM, Tamis) and mixed in different proportions in a ball mill (Yamato, UB 32) at approximately 400 rpm for about 3 h.

After milling, the mixtures were subjected to uniaxial pressing at 400 MPa for 10 seconds (VEB, Werkstoffprüfmaschinen Leipzig) in a mold with an approximate diameter of 1 cm. The green specimens were placed in a standard furnace (ME-1700) for a sintering cycle of 8 °C/min up to 600 °C, with a dwell time of 2 h to remove the binder from the ZrO_2-Y_2O_3. After the binder removal period, the specimens were heated at a rate of 8 °C/min up to 800 °C, followed by 5 °C/min up to 1200 °C, and then at a heating rate of 3 °C/min from 1200 °C to 1400 °C, remaining at this temperature for 5 h.

Table 1. Studied Compositions.

Specimens	3Y-TZP – Tosoh					
	ZrO_2		Y_2O_3		Nb_2O_5(*)	
	wt%	mol%	wt%	mol%	wt%	mol%
0Nb-ZY	94,80	97,00	5,20	3,00	0,00	0,00
1Nb-ZY	93,85	96,63	5,15	2,89	1,00	0,48
3Nb-ZY	91,96	95,69	5,04	2,86	3,00	1,44
5Nb-ZY	90,06	94,74	4,94	2,83	5,00	2,43
7Nb-ZY	88,16	93,75	4,84	2,81	7,00	3,34
10Nb-ZY	85,32	92,23	4,68	2,76	10,00	5,01
26Nb-ZY	74,00	85,72	0,0	0,0	26,0	14,28

(*) Same concentration for all different polymorphs.

The composition that remained intact during the first stage was selected. As will be presented in the Results and Discussion section, this was composition 1Nb-ZY, as shown in Table 1. At this stage, the monoclinic Nb_2O_5 CBMM was subjected to milling in a high-energy mill at 200 rpm for 5 h (Fritsch Pulverizette 5) to achieve a finer granulometry. This procedure was performed to obtain a system with greater homogeneity in the oxide mixture. In this context, the oxide mixing process was carried out dry, where the reagents were first sieved using a 320-mesh sieve, then mixed in well-defined portions using a ball mill rotating at approximately 400 rpm (YAMATO, UB 32) with alumina spheres for about 3 h. The mixtures were subjected to uniaxial pressing at 100 MPa for 10 s (EMIC, DL Line), followed by cold isostatic pressing at 250 MPa for 60 s (AIP, CP360). The green specimens were placed in a standard furnace (ME-1700-INTE) for a sintering cycle of 8 °C/min up to 600 °C, with a dwell time of 2 hours to eliminate organic elements. After the binder removal period, the specimens were heated at a rate of 8 °C/min up to 800 °C, followed by 5 °C/min up to 1200 °C, and then at a heating rate of 3 °C/min from 1200°C to 1400 °C, remaining at this temperature for 1 hour.

Characterizations

X-Ray Diffraction and Raman Spectroscopy: The raw materials and sintered specimens were characterized by X-ray diffraction (Shimadzu XRD 6000, using Co and Cu Kα radiation) with a scanning rate of 1°/min in the range of 20° to 80°. For the 1Nb-ZY specimens, both before and after aging, specimens measuring 1 cm × 1 cm were used. Raman spectroscopy analyses were performed using a Witec 300-R confocal system with a 532 nm wavelength laser and a power of 1 mW.

Scanning Electron Microscopy: The raw materials and sintered specimens were analyzed by scanning electron microscopy (Quanta 400 FEG Zeiss) in secondary electron mode with an acceleration voltage of 20 kV.

Flexural Strength: The test was based on ASTM C1161 – 18 (Standard Test Method for Flexural Strength of Advanced Ceramics at Ambient Temperature) [22]. This method covers the determination of the bending strength of advanced ceramic materials at ambient temperature (Instron, 3369). In this type of test, the specimen is positioned appropriately and subjected to an increasing load at a constant speed until it fractures. In this test, 3 contact points were used, with a sample size of 10 specimens, a maximum distance between points of 40 mm, and a speed of 0.5 mm/min. The dimensions of the specimens followed those specified by the ASTM C1161 – 18.

Apparent Density: The apparent density measurements were carried out based on the method described in ASTM C 20 (Standard Test Methods for Apparent Porosity, Water Absorption, Apparent Specific Gravity, and Bulk Density of Burned Refractory Brick and Shapes by Boiling Water) [23]. In this context, the specimens were placed in an oven (Nova Ética) and then subjected to boiling distilled water using a heating plate (IKA, RH Basic 2) for 2 h. The dry masses, wet masses, and immersed masses were measured using an analytical balance adapted for the Archimedes method (Mettler Toledo, AB204-S/FACT).

Microhardness: It was measured using standard equipment (EQUILAM, HVS-1000) with a force of 0.981 N applied in normal force for a duration of 15 s (SWAB, 2011). The analysis of the indentation dimensions was performed using the equipment's software. These measurements were conducted in accordance with ASTM C1327 – 15 (Standard Test Method for Vickers Indentation Hardness of Advanced Ceramics) [24].

Accelerated Aging: This test promotes accelerated aging of ceramic specimens by placing them in an autoclave (temperature of 134°C, pressure of 0.2 MPa for 5 h) (PHOENIX, AB25). This process standardizes that each hour in the autoclave is equivalent to 4 years in an in vivo system at a temperature of 37 °C [25].

In vitro cytotoxicity evaluations: ISO 10993-5 (INTERNATIONAL ORGANIZATION for STANDARDIZATION. ISO 10993-5. Biological evaluation - Part 5: Test for in vitro cytotoxicity, 2009). In this analysis, indirect cytotoxicity on extracts and direct cytotoxicity on specimens were considered. Parameters: Cell line: L929 (ATCC No. CCL1, NCTC clone 929L); Culture Medium: DMEM (Sigma) containing 10% Bovine Fetal Serum (Sigma); Negative Cytotoxicity Control: filter paper discs; Positive Control of Cytotoxicity: latex glove discs [26].

Results

Characterization of the Raw Material: The analysis using SEM showed powders with different particle size distributions, which can be observed in Figures 1, 2, and 3.

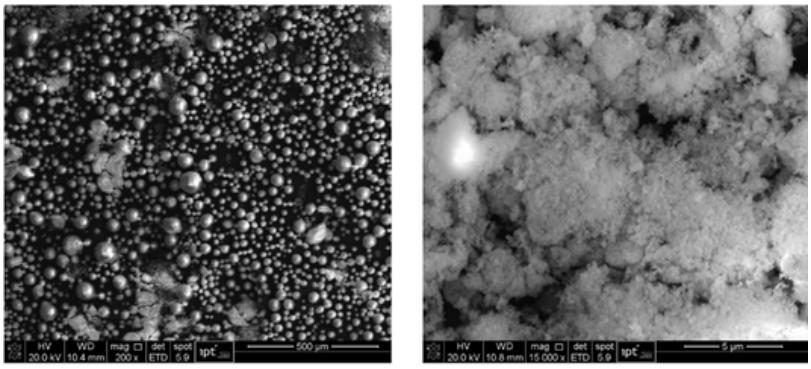

Figure 1. Powders from zirconium oxide manufactured by the company Tosoh and commercially named TZ-3YSB-E.

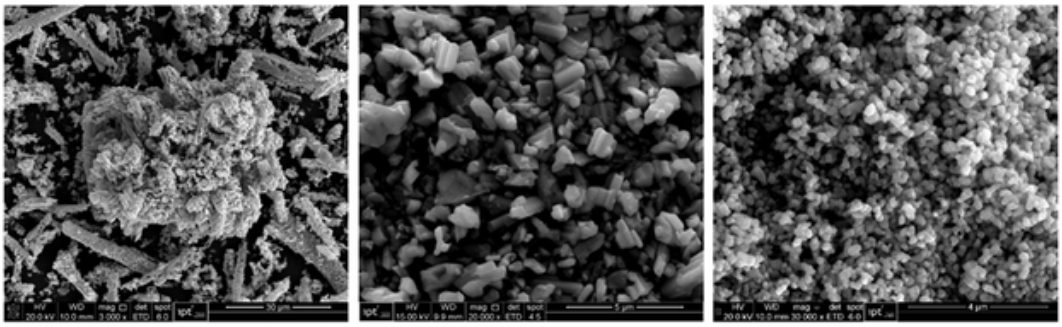

Figure 2. Powders from niobium oxide manufactured by CBMM and Merck and presented according to the type of polymorph present.

The characterization of the powders shown in Figure 2 was also performed by X-ray diffraction to understand not only the degree of purity of the specimens but also to validate information provided by the manufacturers and existing literature.

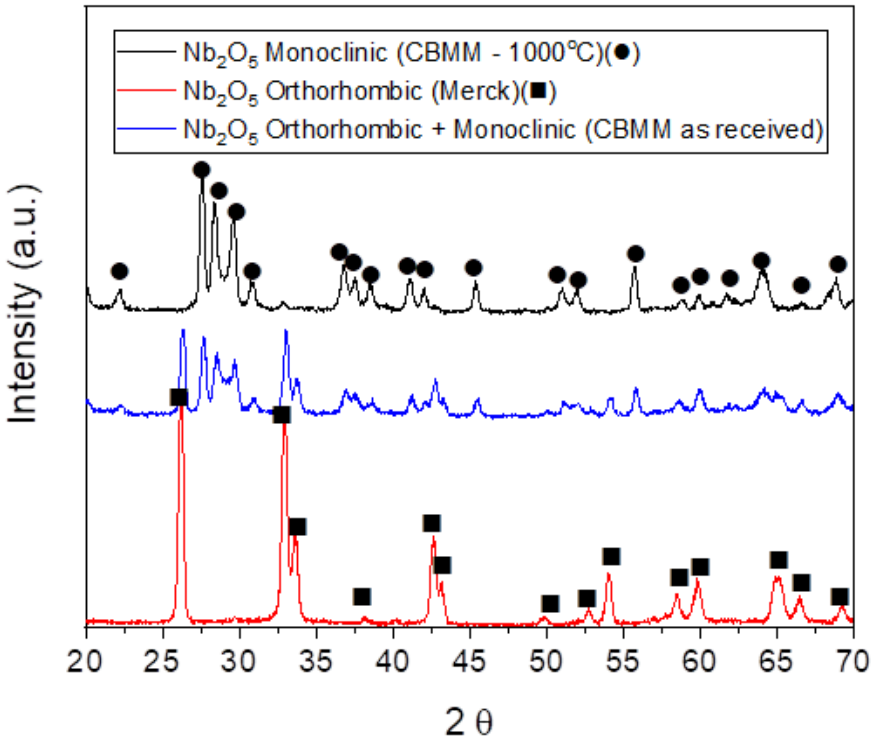

Figure 3. X-ray diffraction of the niobium oxide powders.

Visual analysis of the anisotropy coefficient of Nb_2O_5: Manning et al. reported the thermal coefficient anisotropy of monoclinic Nb_2O_5 [18]. According to these authors, the difference in the expansion coefficient in the **a** ($5.3x10^{-6}$/°C), **b** (0) and **c** ($5.9x10^{-6}$/°C) of the crystal structure of monoclinic niobium oxide leads to the formation of microcracks in the sintered body of this material.

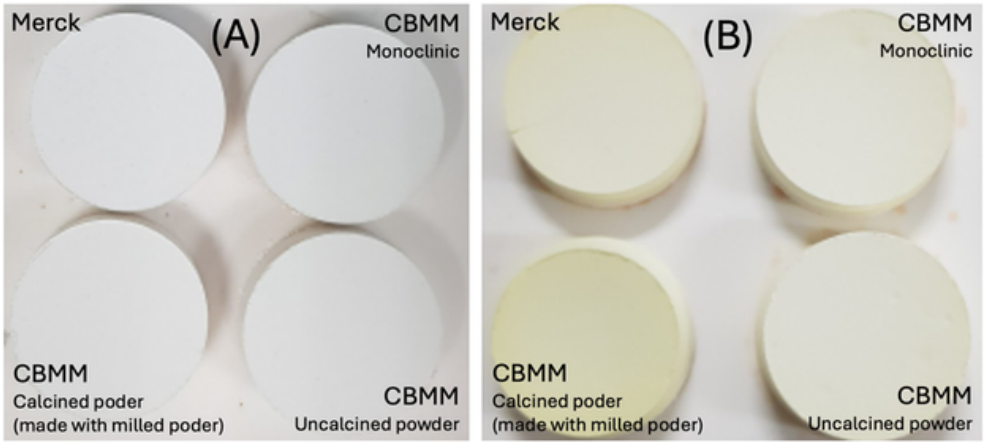

Figure 4. (A) Green Nb_2O_5 pellets and (B) pellets sintered at 1400°C/1h.

The groups of sintered specimens, showed in Figure 4, were subjected to SEM analysis in order to investigate the presence of microcracks. These observations were conducted on the flat surface of the specimens as presented in Figure 5.

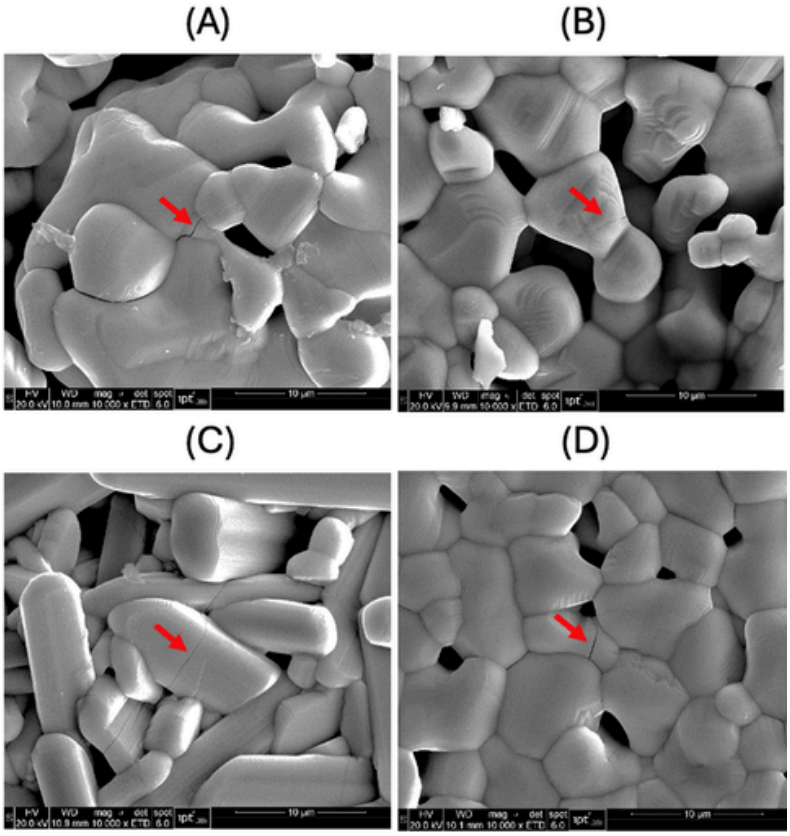

Figure 5. SEM micrographs of the Nb_2O_5 pellets sintered at a maximum temperature of 1400 °C/1 h. (A) surface of specimens from monoclinic and orthorhombic polymorphs (B) only monoclinic (C) only monoclinic pulverized after calcination and (D) only orthorhombic. Source: Developed by the author.

The formation of microcracks without the fracture of the specimens is possible through the understanding of the phenomenon common to its class as a polycrystalline ceramic material. During the cooling of Nb_2O_5 from the sintering temperature, unequal contraction of the crystals occurs, generating internal stresses. These stresses are more pronounced in directions with high thermal expansion coefficients (directions a and c) and compressive in directions with low coefficients (direction b). When these stresses exceed the strength of the crystals or the bonds between them, internal fracture occurs, leading to the formation of microcracks [18].

The presence of microcracks causes anomalous thermal expansion, or even contraction, at lower temperatures. Initially, the individual thermal expansion of the crystals is accommodated by the cracks, preventing the body from expanding as a whole. As the temperature increases, the fracture surfaces begin to recombine, resulting in the expansion of the body [18, 27-28].

The hysteresis observed during the heating and cooling cycles of sintered specimens can be attributed to the occurrence and recombination of microcracks. Therefore, an inversely proportional relationship between the density of microcracks and porosity is observed, a characteristic that may explain the maintenance of the macrostructure of the developed specimens, even in the presence of microcracks. These specimens were developed with grain sizes and compaction profiles of the green specimens in such a way as to be less susceptible to catastrophic fractures [18].

Developing specimens based on ZrO_2-Y_2O_3-Nb_2O_5 system: Based on the understanding of the sintering behavior of Nb_2O_5, the process of forming specimens containing ZrO_2 (manufacturer TOSOH with product described as TZ-3YSB-E) and Nb_2O_5, with different polymorph configurations, was initiated. Table 2 presents the developed profiles and the identification of catastrophic failures after the sintering process.

Table 2 - Relationship between the type of Nb_2O_5 polymorph, polymorph content, and integrity of sintered specimens of the TZ-3YSB-E-Nb_2O_5 system after cooling.

Nb_2O_5 Polymorph Type	Mass Fraction of Nb_2O_5 and ZrO_2 (Tosoh) [wt%]	Fracture Profile	Nomenclature
Monoclinic	1-99	**Intact**	TZ-3YSB-E _1M
	3-97	Partial Fracture	
	5-95	Partial Fracture	
	7-93	Total Fracture	
	10-90	Total Fracture	
	26-74	**Intact**	
Polymorph Mixture	1-99	**Intact**	TZ-3YSB-E _1MO
	3-97	Partial Fracture	
	5-95	Total Fracture	
	7-93	Total Fracture	
	10-90	Total Fracture	
Orthorhombic	1-99	**Intact**	TZ-3YSB-E _1O
	3-97	Partial Fracture	
	5-95	Total Fracture	
	7-93	Total Fracture	
	10-90	Total Fracture	

Among the sintered specimens that remained intact, those containing 1% and 26% Nb_2O_5 were identified. In contrast, the remaining specimens exhibited partial or complete fractures immediately after the proposed thermal cycle. Studies on the $26Nb_2O_5$-$74ZrO_2$ [wt%] system suggest the formation of the $Zr_6Nb_2O_{17}$ [28-29]. The differences in integrity levels can be observed in Figure 6.

Under appropriate conditions, the formation of a specific crystalline structure of $Zr_6Nb_2O_{17}$ occurs instead of a mixture of individual oxides. This structure exhibits an orthorhombic arrangement, allowing zirconium and niobium atoms to bond stably through oxygen linkages, forming a crystalline lattice. Additionally, the interaction between niobium and zirconium atoms, facilitated by Nb-O-Zr bonds, is fundamental to the material's stability. These bonds promote a cohesive three-dimensional network, preventing the separation of components into distinct phases [28, 30].

In other words, the structure of $Zr_6Nb_2O_{17}$ is described as a superstructure composed of metal and oxygen subcells, which accommodate different concentrations of Nb. This structural accommodation capability contributes to the material's stability. Finally, when stoichiometric molar ratios are used, X-ray diffraction analysis reveals the formation of a single $Zr_6Nb_2O_{17}$ phase, with no evidence of other oxides [31-33].

From the perspective of ionic interactions, the addition of Nb_2O_5 to yttria-stabilized zirconia modifies the densification mechanisms primarily through the generation of $Nb^{5+}\rightarrow Zr^{4+}$ substitutional defects, which increase the concentration of oxygen vacancies and enhance the anionic diffusion responsible for the initial stages of sintering. This effect may be further reinforced by the formation of small amounts of eutectic phases or transient liquids that lower the onset temperature of densification and accelerate pore closure [34–36]. Furthermore, Nb^{5+} doping can promote grain-boundary solute drag, supporting high densification while limiting excessive grain growth [37].

Regarding phase stability, Nb^{5+} tends to destabilize the tetragonal phase of zirconia because the oxygen vacancies generated by pentavalent doping do not stabilize tetragonality as effectively as those associated with Y^{3+}. Increased ionic disorder and lattice distortion decrease the free energy of the tetragonal phase, thereby facilitating the martensitic tetragonal→monoclinic transformation during cooling or under mechanical stress [1, 38-39]. Thermodynamically, the higher defect density reduces the energetic barrier for this transformation, making the material more susceptible to phase change [40].

Thus, Nb_2O_5 exerts a dual influence on the ZrO_2–Y_2O_3 system: it accelerates densification by increasing diffusional mobility during sintering, while simultaneously reducing tetragonal stability by altering defect equilibria and structural symmetry. These phenomena directly affect the final microstructure and the mechanical properties of zirconia-based biomedical ceramics [41,42].

Figure 6 - Photographs of sintered ceramic specimens based on their integrity levels (examples from the sintered samples). (A) Intact (TZ-3YSB-E _1M). (B) Partial fracture (3-97 [%wt] with monoclinic Nb_2O_5). (C) Total fracture (10-90 [%wt] with monoclinic Nb_2O_5). Sintered from green specimens diameter: 11 mm.

Densification: Based on the experimental results obtained, it is understood that the experimental density was 6.04 ± 0.01 g/cm³, a value statistically identical to the theoretical one. This high degree of densification suggests that, even with the potential formation of microcracks due to thermal mismatch associated with Nb_2O_5-rich residual regions, part of the oxide distributed within the system may have reacted with the zirconia matrix or formed secondary phases, thereby reducing the extent of microcracking during cooling. Because such possible secondary compounds often exhibit more isotropic thermal behavior, their presence may contribute to maintaining the high densification observed. Furthermore, the resulting grain size, mixing methodology, and pressing conditions may have collectively favored the consolidation of specimens achieving approximately 99% of the theoretical density.

This densification mechanism can be rationalized by the defect chemistry introduced by Nb^{5+} into the zirconia lattice. When incorporated substitutionally into Zr^{4+} sites, Nb^{5+}, whose ionic radius (~0.64–0.69 Å) is slightly smaller than that of Zr^{4+} (0.72 Å), induces local lattice distortions and charge-compensating defects, such as cation vacancies, which can modify species mobility during sintering. These defect structures may enhance mass transport at specific temperatures and promote pore elimination, thus aiding densification in Nb_2O_5-doped zirconia systems. Additionally, niobium redistribution along grain boundaries can alter grain growth kinetics and diffusion pathways, contributing to the sintering behavior reported in the literature for similar ZrO_2–Nb_2O_5–Y_2O_3 ceramic systems [43-44].

Microstructure: Figure 7 presents scanning electron microscope (SEM) images of the TZ-3YSB-E sintered specimens containing 1% of Nb_2O_5 with different types of polymorphs. The microstructure is finer for the compositions without Nb_2O_5 (0% addition) and with 1% Nb_2O_5 from Merck, attributed to their finer granulometry compared to that of the Nb_2O_5 from CBMM. Figure 8 displays micrographs of the fractured surface of TZ-3YSB-E sintered specimens s containing 10% of monoclinic Nb_2O_5, highlighting the cracks that were developed during cooling due to the destabilization of partially stabilized ZrO_2-Y_2O_3. The X-ray diffraction results shown in Figure 9 indicate that the tetragonal phase decreases as the concentration of Nb_2O_5 increases to 10 wt% leading to destabilization of partially stabilized zirconia. However, when the ZrO_2:Nb_2O_5 ratio is set at 6:1, the compact is intact due to the formation of $Zr_6Nb_2O_{17}$.

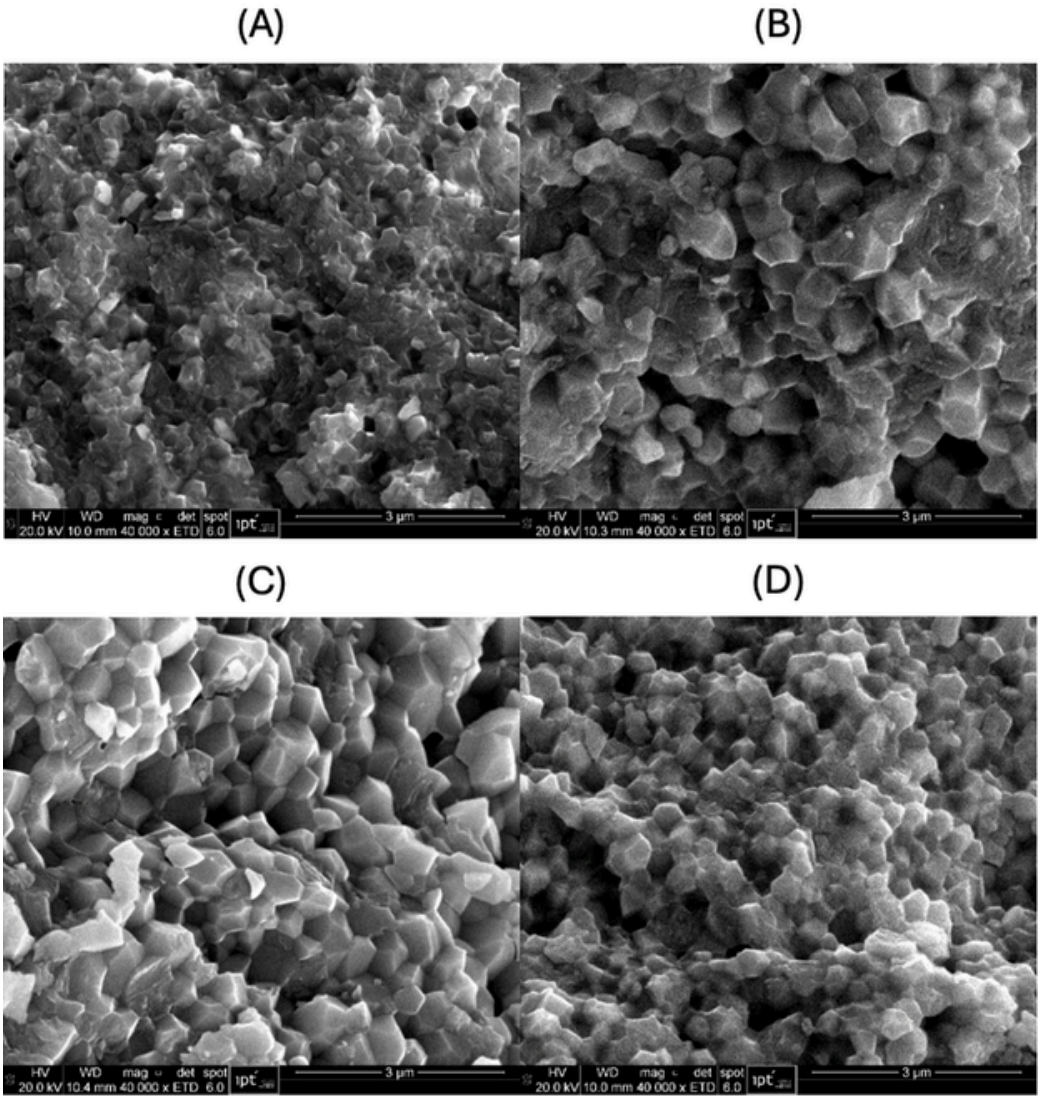

Figure 7 - Fracture surface of specimens of (A) TZ-3YSB-E, (B) TZ-3YSB-E with 1%Nb_2O_5 Monoclinic phase (CBMM), (C) TZ-3YSB-E with 1%Nb_2O_5 Monoclinic and Orthorhombic phases (CBMM), and (D) TZ-3YSB-E with 1%Nb_2O_5 Orthorhombic phase (Merck).

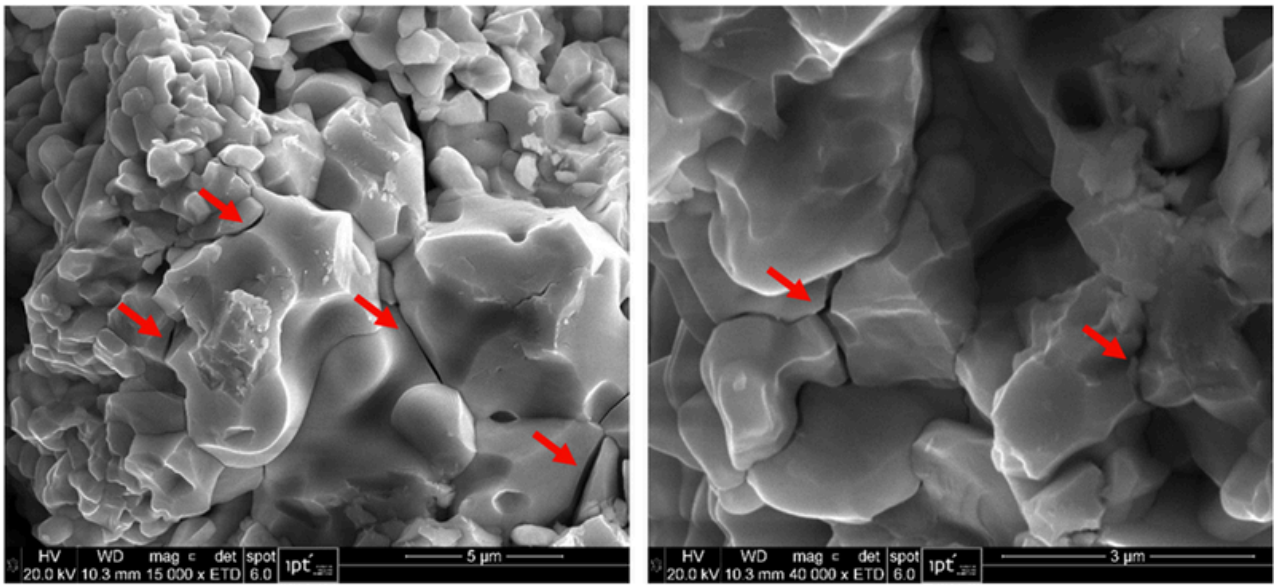

Figure 8 - SEM micrographs of the fracture surface of pellets composed by 90 wt% TZ-3YSB-E and 10 wt% Nb_2O_5 monoclinic phase that was sintered at 1400 °C/1h.

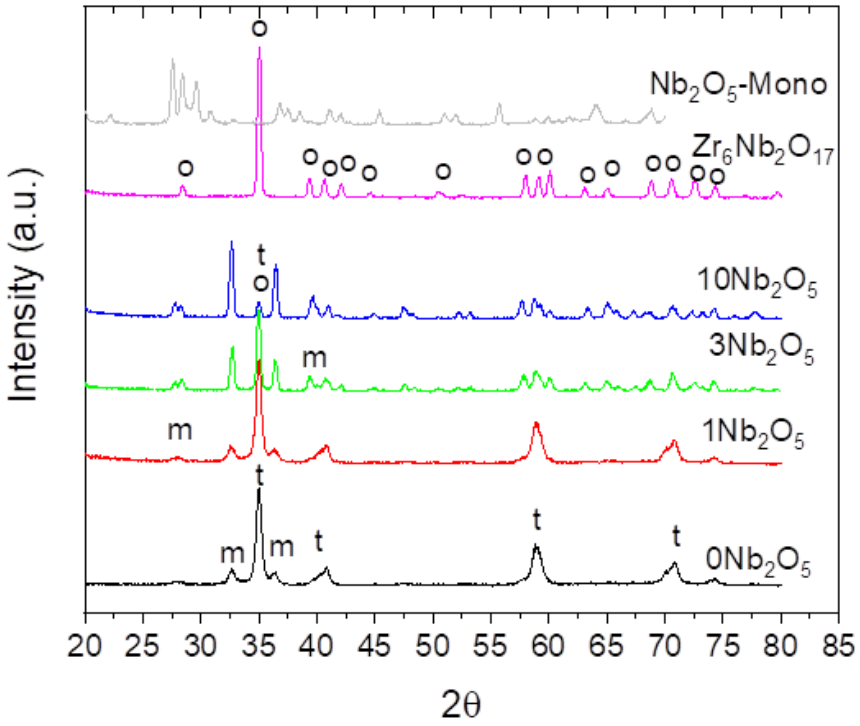

Figure 9 -X-ray diffractograms of pellets with different systems of TZ-3YSB-E and monoclinic Nb_2O_5 (CBMM). The concentrations where 0 wt% Nb_2O_5 ($0Nb_2O_5$), 1 wt% Nb_2O_5 ($1Nb_2O_5$), 3 wt% Nb_2O_5 ($3Nb_2O_5$), 10 wt% Nb_2O_5 ($10Nb_2O_5$), 26 wt% Nb_2O_5 ($Zr_6Nb_2O_{17}$), and only monoclinic Nb_2O_5. Radiation of Co Kα.

Figure 10 shows the Raman spectra of compacts prepared with 0.0, 1.0, and 10.0 wt% of Nb_2O_5 from CBMM (monoclinic). In the specimen containing 10 wt% Nb_2O_5 (equivalent to 5.01 mol%), the tetragonal phase was not observed, indicating a complete destabilization of the zirconia tetragonal phase. Although the band at 811 cm^{-1} is quite weak, it suggests the presence of $YNbO_4$, as reported by Kim et al. [45]. The band located around 780 cm^{-1} is attributed to the Nb-O bond within the ZrO_2-Y_2O_3-Nb_2O_5 system, as noted by Lee, Jang, and Kim and Tan et al.[21, 46].

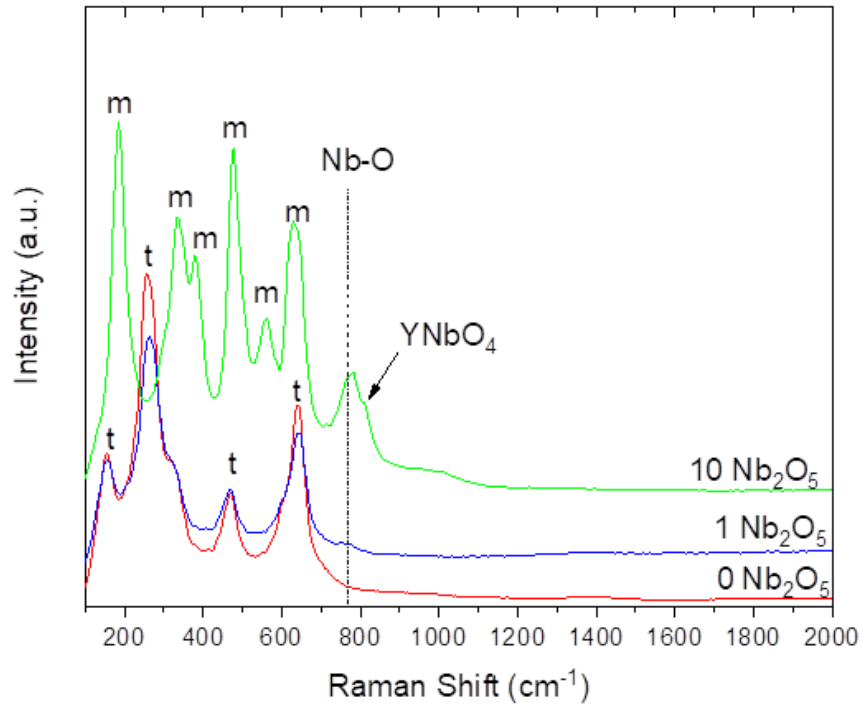

Figure 10 - Raman spectra of pellets with different systems of TZ-3YSB-E and monoclinic Nb_2O_5 (CBMM). The concentrations where 0 wt% Nb_2O_5 ($0Nb_2O_5$), 1 wt% Nb_2O_5 ($1Nb_2O_5$), and 10 wt% Nb_2O_5 ($10Nb_2O_5$).

Microhardness: The Vickers microhardness value measured for sintered specimens composed by TZ-3YSB-E with 1 wt% of monoclinic Nb_2O_5 (CBMM) resulting in approximately (10.010 ± 0.355) GPa. Although these values are lower than those of commercial Y-TZP, they were not found to be significantly different in practice, falling within 70.30% to 77.72% of the performance reported in the literature [47-48]. In addition to these findings, a deeper examination of the statistical significance of the microhardness results is essential to properly contextualize their mechanical relevance. Although the measured mean value and relatively narrow standard deviation suggest consistent experimental response, reliance solely on the absence of statistical differences may mask subtle but functionally important variations, especially in advanced ceramics where microstructural heterogeneity strongly influences hardness behavior. In zirconia-based systems, factors such as grain boundary chemistry, dopant distribution, and residual stress fields can generate local hardness fluctuations that are not captured when only P-values are considered [49–51]. Complementary metrics, such as effect size, confidence intervals, and intra-sample variability analyses, provide a more comprehensive framework for determining whether the observed differences could influence wear resistance or long-term reliability, even when they fall below conventional thresholds of statistical significance. Previous studies have shown that small changes in hardness, though statistically non-significant, may meaningfully alter mechanical response under cyclic loading or contact fatigue in biomedical applications [52]. Incorporating these broader descriptors therefore enhances the interpretation of the microhardness findings and aligns the analysis with best practices in ceramic materials characterization.

Accelerated Aging: As illustrated in Figure 11, there was an average reduction of about 20% in the strength of the aged (654.19 ± 83.52 MPa) compared to the non-aged specimens (787.16 ± 116.53 MPa). This reduction can be attributed to the transformation of tetragonal to monoclinic zirconia. Figure 12 indicates that the intensity of the peak at 28.15° corresponding to monoclinic ZrO_2 is more pronounced in the compact aged at134 °C for 5 h. This finding suggests that the addition of 1 mol% Nb_2O_5 (from CBMM - monoclinic) influences the transformability of zirconium oxide in our study. Lee et al. [9] investigated the effects of adding Nb_2O_5 and Y_2O_3 on the aging of ZrO_2. They found that the m→t phase transformation did not occur in a composition containing 90.24 mol% ZrO_2, 5.31 mol% Y_2O_3, and 4.75 mol% Nb_2O_5, even when aged in the temperature range of 200 °C to 400 °C for up to 1000 h. The authors suggest that the retention of low-temperature degradation (LTD) rates is due to the balancing of charge neutrality, facilitated by the replacement of Nb^{5+} and Y^{3+} ions for Zr^{4+} ions. The control of stabilization and LTD in zirconium oxide, which is partially or fully stabilized by Y_2O_3, relies on several factors. These include grain size, tetragonality (c/a), the amount of additive (in this case, Nb^{5+}), charge balancing, vacancy annihilation, and the formation of NO_4, YO_8, and ZrO_8 units. These factors are critical in managing the internal stresses responsible for the m-t transformation [9, 13-14, 17, 53]. In our study, given the molar ratios used, the selected raw materials, and the resulting microstructure, we found that equilibrium conditions were not achieved.

In addition to these observations, a more detailed examination of the statistical significance of the flexural strength results is essential for a complete interpretation of the material's mechanical behavior. Although the average reduction of approximately 20% in flexural strength between non-aged and aged specimens appears substantial, the relatively high standard deviations associated with both

conditions (116.53 MPa and 83.52 MPa, respectively) indicate considerable data dispersion, which may reduce the statistical power of conventional hypothesis-testing. Ceramics such as Y-TZP and Nb_2O_5-doped zirconia often exhibit variability arising from microstructural heterogeneities, including flaw population, grain size distribution, and local phase assemblages, that can influence fracture behavior without necessarily producing statistically significant differences when evaluated solely by P-values [54–56]. Complementary analyses such as effect size, Weibull modulus evaluation, confidence intervals, and probability-of-failure modeling provide a deeper understanding of whether the observed reductions in strength reflect true mechanical degradation or fall within the variability expected for polycrystalline ceramic systems [57]. Incorporating these statistical descriptors would therefore enhance the robustness of the interpretation and allow the mechanical implications of aging and phase transformation to be more accurately contextualized.

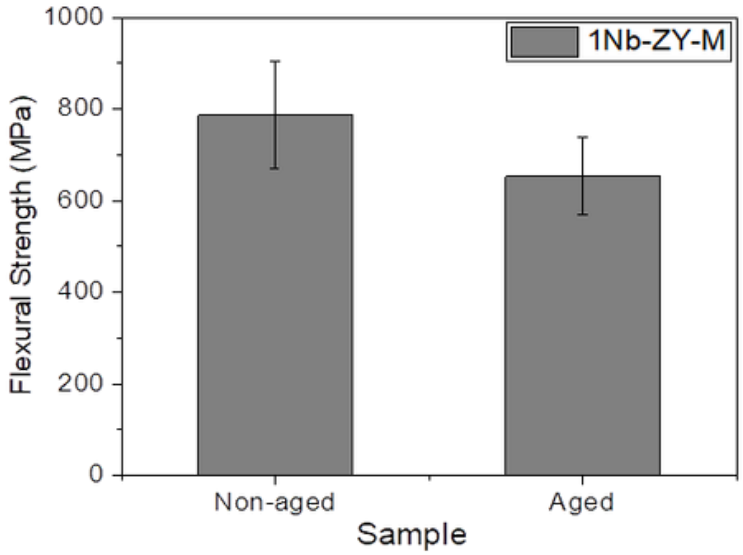

Figure 11 - Flexural strength of the sintered specimens composed by TZ-3YSB-E with 1 wt% of monoclinic Nb_2O_5 from CBMM (1Nb-ZY-M) before and after aging.

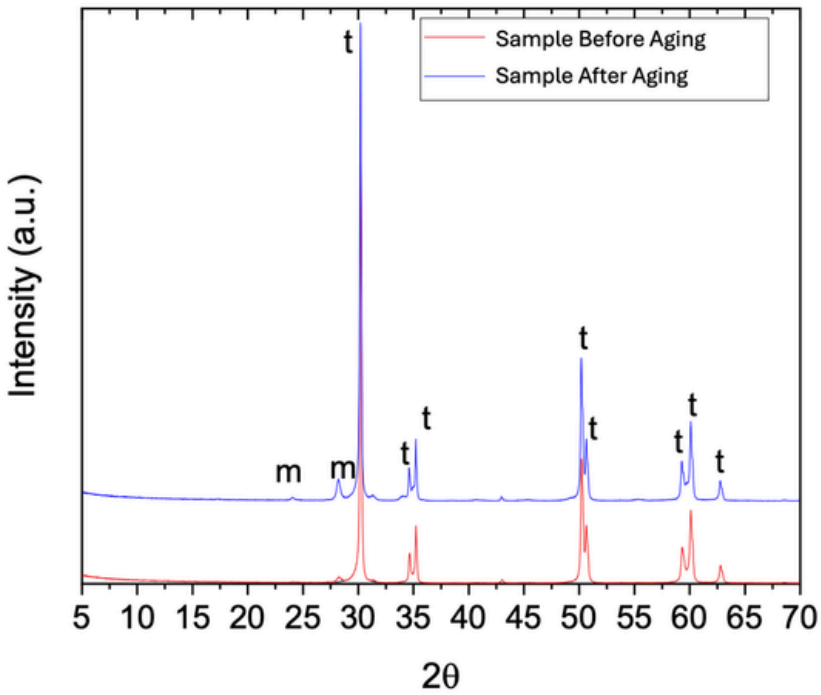

Figure 12 - X-ray diffractograms of the sintered specimens composed by TZ-3YSB-E with 1 wt% of monoclinic Nb_2O_5 from CBMM before and after aging.

Cytotoxicity: Although zirconia-based ceramics are generally considered bioinert, there are limited studies on the ZrO_2-Y_2O_3-Nb_2O_5 system concerning this important material property. Pradham et al [58]. investigated cell viability using L-929 fibroblast cell lines for implants coated with Nb_2O_5 and TiO_2. Their findings indicated that cell viability was higher for the TiO_2-coated samples (122%) compared to the growing cell population. In contrast, the implants coated with Nb_2O_5 showed variable viability, ranging from 64% to 105%, which was partly dependent on the atomic structure of the materials. Specifically, the authors found that hexagonal Nb_2O_5 demonstrated bioactivity, whereas amorphous and orthorhombic forms did not. However, the study did not include an analysis of monoclinic Nb_2O_5 [58-63]. Obata et al. [64] demonstrated that exposure of osteoblastic cells to Nb^{5+} ions released from niobium-containing bioactive materials did not compromise cell viability or morphology; on the contrary, the authors reported maintenance of metabolic activity and even increased osteogenic markers, such as alkaline phosphatase activity and matrix mineralization. Additionally, although Dsouki et al. [65] primarily evaluated systemic biological responses in vivo, their findings also support the notion of low biological reactivity and the absence of adverse cellular effects attributable to niobium-based compounds. Collectively, these observations reinforce that Nb_2O_5, even when incorporated into zirconia-based ceramics, is unlikely to induce cytotoxic responses under typical extract test conditions. Such results further support the relevance of cytotoxicity analysis for ZrO_2–Y_2O_3–Nb_2O_5 systems.

In this study, it is observed the cell monolayer both macroscopically and microscopically after 24 hours of exposure to the test materials. The control (TZ-3YSB-E) and specimens made by TZ-3YSB-E with 1 wt% of monoclinic Nb_2O_5 from CBMM showed a reactivity degree of 0 (n = 3), indicating that there were no alterations in the cells compared to the negative control. The validation of the test was confirmed by the presence of an inhibition halo and cellular changes around the latex sample, which served as a positive control for cytotoxicity. These results are illustrated in Figures 13 and 14. Additionally, Figure 15 displays the positive control (A), the negative control (B), and a well without any interference (C).

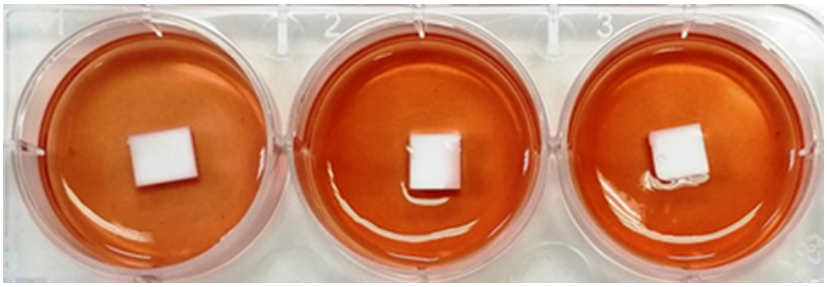

Figure 13 - Presentation of the wells containing the control specimen (TZ-3YSB-E). L929 cell line culture submerged in the agar layer containing approximately 1 cm² of specimen placed above.

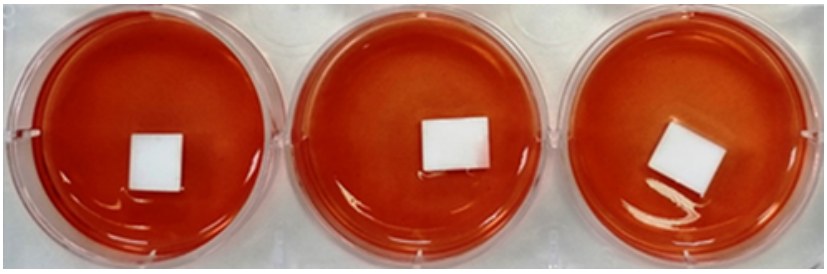

Figure 14 - Presentation of the wells containing the sintered specimens composed by TZ-3YSB-E with 1 wt% of monoclinic Nb_2O_5 from CBMM. L929 cell line culture submerged in the agar layer containing approximately 1 cm² of specimens allocated above.

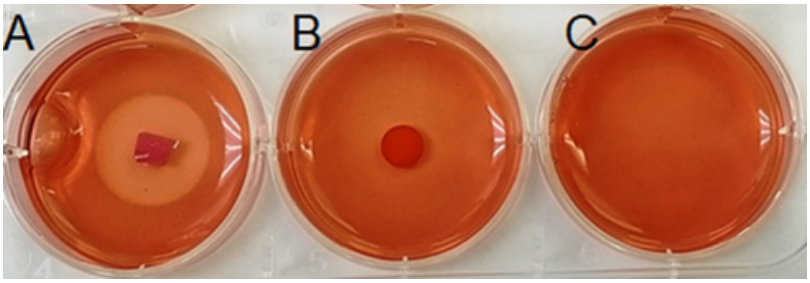

Figure 15 - L929 cell line culture submerged in an agar layer containing approximately 1 cm² of sample placed on top. A = positive/cytotoxic control. B = negative/non-cytotoxic control. C = well containing cells without interaction.

The quantitative test results, obtained by performing serial dilutions in base 2 of the extracts from the sintered specimens composed by TZ-3YSB-E with 0, 1 and 26 wt% of monoclinic Nb_2O_5 from CBMM indicated no cytotoxicity towards the reference cells used in the experiment, as shown in Figure 16. All conditions demonstrated a cell viability of 100% or higher. The P-value for the analysis of variance was 0.151, which is greater than 0.05 and suggests that there is no statistical evidence to indicate that the means are different.

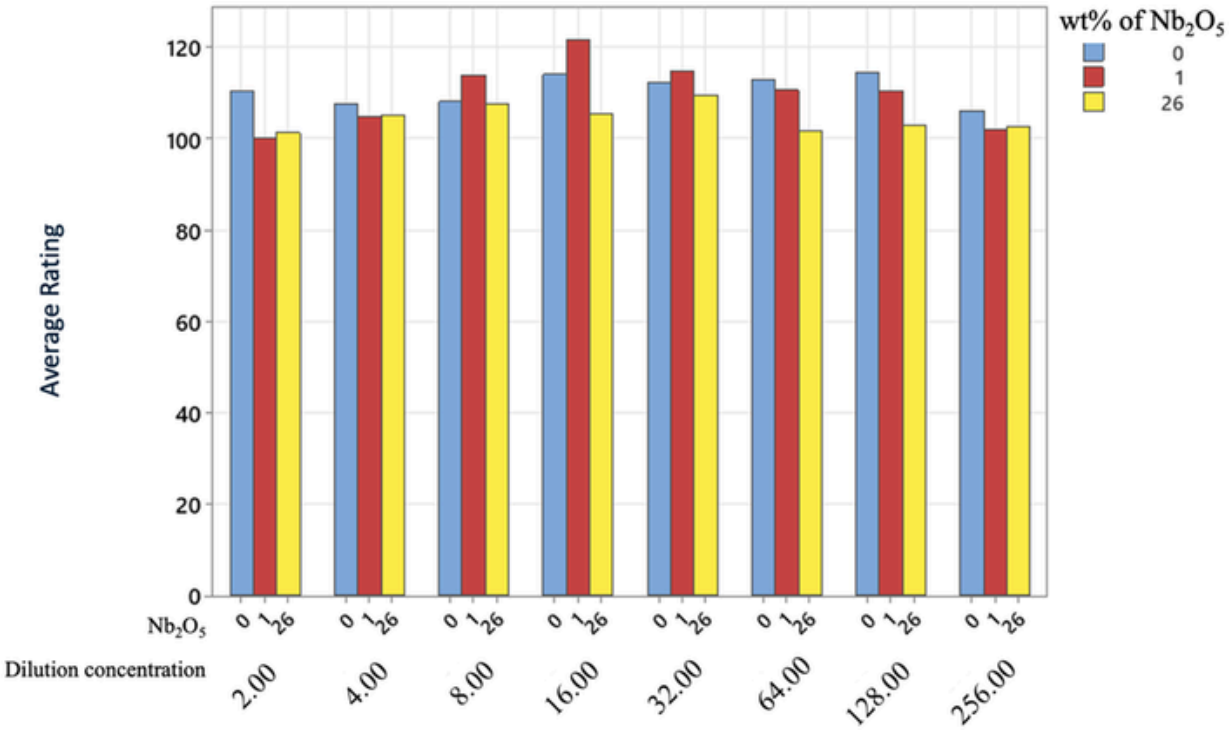

Figure 16 - Analysis of variations in cell viability percentages of the sintered specimens composed by TZ-3YSB-E with 0 (0), 1 (1) and 26 (26) wt% of monoclinic Nb_2O_5 from CBMM control samples as a function of increasing dilution at level 2.

Conclusions

According to the study on the addition of different polymorphs in the ZrO_2-Y_2O_3 system with 3 mol% concentration, and considering the molar ratios of Nb_2O_5/Y_2O_3, the chosen raw materials, and the procedural conditions, the following conclusions can be drawn:

- The Nb_2O_5 compacts exhibited microcracks in their microstructure after heat treatment and cooling from 1400 °C to 25 °C,
- The addition of up to 1% by weight of Nb_2O_5 resulted in intact compacts, regardless of the Nb_2O_5 polymorph used,

- The addition of 3% to 10% by weight led to fractured compacts after heat treatment and cooling, independent of the Nb_2O_5 polymorph used in the formulations,
- The densification of the compacts was higher than 99% at 1400 ºC /1 h,
- The hardness of the ZrO_2-Y_2O_3 system with 1% of monoclinic Nb_2O_5 was (10.010 ± 0.355) GPa,
- The flexural strength of the sintered ZrO_2-Y_2O_3 compact with 1% monoclinic Nb_2O_5 decreased from (787.16 ± 116.53) MPa to (654.19 ± 83.52) MPa after aging. This reduction indicates a transformation from tetragonal to monoclinic (t→m), as observed through X-ray analyses,
- The cell viability and proliferation studies indicated that none of the specimens exhibited cytotoxicity following the addition of monoclinic Nb_2O_5 to ZrO_2-Y_2O_3.

References

[1]. Hannink RHJ, Kelly PM, Muddle BC. Transformation toughening in zirconia-containing ceramics. J Am Ceram Soc. 2000;83:461-87. Available from: https://doi.org/10.1111/j.1151-2916.2000.tb01221.x

[2]. Benalcázar-Jalkh EB, Campos TMB, Santos C, Alves LMM, Carvalho LF, Bergamo ETP, Tebcherani SM, Witek L, Coelho PG, Thim GP, Yamaguchi S, Sousa EO, Marcolino GA, Bonfante EA. Novel bilayered zirconia systems using recycled 3Y-TZP for dental applications. Dent Mater. 2025;41:402-13. Available from: https://doi.org/10.1016/j.dental.2024.12.013

[3]. Imariouane M, Saâdaoui M, Denis G, Reveron H, Chevalier J. Aging behavior of a 1.5 mol% yttria doped zirconia exhibiting optimized toughness and strength. J Eur Ceram Soc. 2024;44:1053-60. Available from: https://doi.org/10.1016/j.jeurceramsoc.2023.09.041

[4]. Garvie RC, Hannink RHJ, Pascoe RT. Ceramic steel? Nature. 1975;258:703-4. Available from: https://www.nature.com/articles/258703a0

[5]. Garvie RC, Nicholson PS. Structure and thermomechanical properties of partially stabilized zirconia in the CaO-ZrO_2 system. J Am Ceram Soc. 1972;55:152-7. Available from: https://doi.org/10.1111/j.1151-2916.1972.tb11241.x

[6]. Bergamo ETP, Cardoso KB, Lino LFO, Campos TMB, Monteiro KN, Cesar PF, Genova LA, Thim GP, Coelho PG, Bonfante EA. Alumina-toughened zirconia for dental applications: Physicochemical, mechanical, optical, and residual stress characterization after artificial aging. J Biomed Mater Res B Appl Biomater. 2021;109:1135-44. Available from: https://doi.org/10.1002/jbm.b.34776

[7]. Chevalier J. What future for zirconia as a biomaterial? Biomaterials. 2006;27:535-43. Available from: https://doi.org/10.1016/j.biomaterials.2005.07.034

[8]. Schubert H, Frey F. Stability of Y-TZP during hydrothermal treatment: Neutron experiments and stability considerations. J Eur Ceram Soc. 2005;25:1597-602. Available from: https://doi.org/10.1016/j.jeurceramsoc.2004.03.025

[9]. Lee DY, Kim DJ, Cho DH, Lee MH. Effect of Nb_2O_5 and Y_2O_3 alloying on the mechanical properties of TZP ceramics. Ceram Int. 1998;24:461-5. Available from: https://doi.org/10.1016/S0272-8842(97)00036-9

[10]. Lim HB, Oh KS, Kwon YJ, Kim YK, Lee DY. Influence of abrasive machining and annealing on hydrothermal stability of zirconia-alumina composites as a hip joint head. Key Eng Mater. 2007;330-332:1223-6. Available from: https://doi.org/10.4028/www.scientific.net/KEM.330-332.1223

[11]. Kim DJ. Effect of Ta_2O_5, Nb_2O_5, and HfO_2 alloying on the transformability of Y_2O_3-stabilized tetragonal ZrO_2. J Am Ceram Soc. 1990;73:115-20. Available from: https://doi.org/10.1111/j.1151-2916.1990.tb05100.x

[12]. Lee DY, Kim DJ, Cho DH. Low-temperature phase stability and mechanical properties of Y_2O_3- and Nb_2O_5-co-doped tetragonal zirconia polycrystal ceramics. J Mater Sci Lett. 1998;1:185-7. Available from: https://doi.org/10.1023/A:1006567808134

[13]. Kim DJ, Jung HJ. Fracture toughness, ionic conductivity, and low-temperature phase stability of tetragonal zirconia co-doped with yttria and niobium oxide. J Am Ceram Soc. 1998;81:2309-14. Available from: https://doi.org/10.1111/j.1151-2916.1998.tb02626.x

[14]. Kim DJ, Jung HJ, Cho DH. Phase transformations of Y_2O_3- and Nb_2O_5-doped tetragonal zirconia during low-temperature aging in air. Solid State Ionics. 1995;80:67-73. Available from: https://doi.org/10.1016/0167-2738(95)00115-M

[15]. Shin JC. Osteogenic potential and reaction to human gingival fibroblasts of (Y, Nb)-zirconia. [dissertation]. Seoul: Seoul National University, Graduate School; 2017. Available from: https://hdl.handle.net/10371/125050

[16]. Souza JVC, Nono MCA, Mineiro SL. ZrO_2–Nb_2O_5 ceramics for application in the aerospace industry. In: Proceedings of the Seventh International Latin American Conference on Powder Technology; 2009 Nov 8-10; Atibaia, Brazil.

[17]. Li P, Chen IW, Penner-Hahn JE. Effect of dopants on zirconia stabilization—an X-ray absorption study: III, charge-compensating dopants. J Am Ceram Soc. 1994;77:1289-95. Available from: https://doi.org/10.1111/j.1151-2916.1994.tb05404.x

[18]. Manning WR, Hunter O Jr, Calderwood FW, Stacy DW. Thermal expansion of Nb_2O_5. J Am Ceram Soc. 1972;55:342-7. Available from: https://doi.org/10.1111/j.1151-2916.1972.tb11306.x

[19]. Pang R, Wang Z, Li J, Chen K. Polymorphs of Nb_2O_5 compound and their electrical energy storage applications. Materials (Basel). 2023;16:6956. Available from: https://doi.org/10.3390/ma16216956

[20]. Pilarek B, Pelczarska AJ, Szczygiel I. Characterization of niobium(V) oxide received from different sources. J Therm Anal Calorim. 2017;127:1-8. Available from: https://doi.org/10.1007/s10973-017-6300-x

[21]. Tan X, Liu C, Luo P, Zhao D, Zhang F. Phase equilibria in the ZrO_2–$YO_{1.5}$–$NbO_{2.5}$ system at 1300 °C and high-temperature experiments in the ZrO_2–$YNbO_4$ subsystem. J Am Ceram Soc. 2025;108:e20175. Available from: https://doi.org/10.1111/jace.20175

[22]. ASTM International. ASTM C1161-18. Standard test method for flexural strength of advanced ceramics at ambient temperature. West Conshohocken (PA): ASTM International; 2018.

[23]. ASTM International. ASTM C20. Standard test methods for apparent porosity, water absorption, apparent specific gravity, and bulk density of burned refractory brick and shapes by boiling water. West Conshohocken (PA): ASTM International; 2015.

[24]. ASTM International. ASTM C1327-15. Standard test method for Vickers indentation hardness of advanced ceramics. West Conshohocken (PA): ASTM International; 2019.

[25]. Chevalier J, Gremillard L. The tetragonal-monoclinic transformation in zirconia: Lessons learned and future trends. J Am Ceram Soc. 2009;92:1901-20. Available from: https://doi.org/10.1111/j.1551-2916.2009.03278.x

[26]. International Organization for Standardization. ISO 10993-5: Biological evaluation of medical devices – Part 5: Tests for in vitro cytotoxicity. Geneva: ISO; 2009.

[27]. Frolov AA, Pavlikov VN, Karpets MV. Thermal expansion of specimens of niobium and tantalum pentoxides obtained by melting in an optical furnace. Refract Ind Ceram. 2007;48:106-10. Available from: https://doi.org/10.1007/s11148-007-0039-zl

[28]. Tsukamoto H. Enhancement of transformation toughening of partially stabilized zirconia by some additives. Ceram Int. 2022;48:20675-89. Available from: https://doi.org/10.1016/j.ceramint.2022.04.047

[29]. Kantcheva M, Budunoglu H, Samarskaya O. Characterization of $Zr_6Nb_2O_{17}$ synthesized by a peroxo route as a novel solid acid. Catal Commun. 2008;9:874-9. Available from: https://doi.org/10.1016/j.catcom.2007.09.015

[30]. Cayirtepe I, Naydenov A, Ivanov G, Kantcheva M. Characterization of niobium-zirconium mixed oxide as a novel catalyst for selective catalytic reduction of NOx. Catal Lett. 2009;132:438-49. Available from: https://doi.org/10.1007/s10562-009-0150-5

[31]. Wen Q, Ma YW, Zhang FL, Sun H, Shang WX, Wang Q, et al. Targeting $Zr_6Nb_2O_{17}$ ceramic material with integrated structure and function: from preparation to performance. Ceram Int. 2023;49:39597-606. Available from: https://doi.org/10.1016/j.ceramint.2023.09.312

[32]. Bai J, Huang Y, Wei D, Fan Z, Seo HJ. Synthesis and characterization of semiconductor heterojunctions based on $Zr_6Nb_2O_{17}$ nanoparticles. Mater Sci Semicond Process. 2020;112:105010. Available from: https://doi.org/10.1016/j.mssp.2020.105010

[33]. Lu D, Lee B, Kondo JN, Domen K. Preparation and characteristics of crystallized mesoporous $Zr_6Nb_2O_{17}$. Micropor Mesopor Mater. 2004;75:203-8. Available from: https://doi.org/10.1016/j.micromeso.2004.07.002

[34]. Rahaman MN. Ceramic Processing and Sintering. 2nd ed. Boca Raton: CRC Press; 2003. Available from: https://doi.org/10.1201/9780203912807

[35]. German RM. Sintering: Theory and Practice. New York: Wiley; 1996. Available from: https://onlinelibrary.wiley.com/doi/book/10.1002/9783527617895

[36]. Feteira A, Dutton S, Sinclair DC, Reaney IM. Phase relations and sintering in Nb-containing zirconia systems. J Eur Ceram Soc. 2012;32(16):4083–4092. Available from: doi:10.1016/j.jeurceramsoc.2012.05.016

[37]. Coble RL. Diffusion models for hot pressing with surface energy and pressure effects. J Appl Phys. 1961;32(5):793–799. Available from: doi:10.1063/1.1736103

[38]. Garvie RC, Nicholson PS. Phase analysis in zirconia systems. J Am Ceram Soc. 1972;55(6):303–305. Available from: doi:10.1111/j.1151-2916.1972.tb11290.x

[39]. Lughi V, Clarke DR. Transformation of tetragonal zirconia grains in 3Y-TZP. Acta Mater. 2005;53(16):5305–5311. Available from: doi:10.1016/j.actamat.2005.07.009

[40]. De Aza AH, Chevalier J, Fantozzi G, Schehl M, Torrecillas R. Crack growth resistance of alumina–zirconia composites. Acta Mater. 2002;50(17):4397–4411. Available from: doi:10.1016/S1359-6454(02)00282-7

[41]. Chiang YM, Birnie D, Kingery WD. Physical Ceramics. New York: Wiley; 1997. Available from: https://onlinelibrary.wiley.com/doi/book/10.1002/9780470316228

[42]. Foresi A, Taveri G, Montanaro L, et al. Sintering and microstructural evolution in ZrO_2–Y_2O_3–Nb_2O_5 ceramics. Ceram Int. 2020;46:11713–11722. Available from: doi:10.1016/j.ceramint.2020.01.245

[43]. Bejugama S, Pandey AK. Effect of Nb_2O_5 on sintering and mechanical properties of ceria stabilized zirconia. J Alloys Compd. 2018;765:1049-54. Available from: https://doi.org/10.1016/j.jallcom.2018.06.280

[44]. Su NK, Rejab NA, Johar B, Sktani ZDI, Ahmad ZA. The influence of niobia additions on microstructure, Vickers hardness and indentation fracture resistance of ZTA ceramic composites. Eng Headway. 2023;15:29-35. Available from: https://doi.org/10.4028/b-Ce5r8T

[45]. Kim M, Ronchetti S, Onida B, Ichikuni N, Fukuoka A, Kato H, Nakajima K. Lewis acid and base catalysis of $YNbO_4$ toward aqueous-phase conversion of hexose and triose sugars to lactic acid in water. ChemCatChem. 2020;12:350-9. Available from: https://doi.org/10.1002/cctc.201901435

[46]. Lee DY, Jang JW, Kim DJ. Raman spectral characterization of existing phases in the ZrO_2-Y_2O_3-Nb_2O_5 system. Ceram Int. 2001;27:291-8. Available from: https://doi.org/10.1016/S0272-8842(00)00079-1

[47]. Coric D, Renjo MM, Curkovic LV. Vickers indentation fracture toughness of Y-TZP dental ceramics. Int J Refract Met Hard Mater. 2017;64:14-19. Available from: https://doi.org/10.1016/j.ijrmhm.2016.12.016

[48]. Tong H, Tanaka CB, Kaizer MR, Zhang Y. Characterization of three commercial Y-TZP ceramics produced for their high-translucency, high-strength and high-surface area. Ceram Int. 2016;42:1077-85. Available from: https://doi.org/10.1016/j.ceramint.2015.09.033

[49]. Zhang Y, Lawn BR. Novel approaches to evaluating the mechanical reliability of dental ceramics. J Dent Res. 2018;97(2):132–40. Available from: https://doi.org/10.1177/0022034517729584

[50]. Kosmac T, Kocjan A, Dakskobler A, Jevnikar P. The relationship between grain-boundary chemistry and mechanical properties in Y-TZP ceramics. Acta Mater. 2019;164:30–41. Available from: https://doi.org/10.1016/j.actamat.2018.10.031

[51]. Deville S, Chevalier J, Gremillard L. Influence of microstructural variability on the mechanical properties of zirconia-based ceramics. Biomaterials. 2006;27(10):2186–92. Available from: https://doi.org/10.1016/j.biomaterials.2005.11.021

[52]. Lughi V, Sergo V. Low-temperature degradation aging of zirconia: a critical review of the relevant aspects in dentistry. Dent Mater. 2010;26(8):807–20. Available from: https://doi.org/10.1016/j.dental.2010.04.006

[53]. Bapat RA, Yang HJ, Chaubal TV, Dharmadhikari S, Abdulla AM, Arora S, Rawal S, Kesharwani P. Review on synthesis, properties and multifarious therapeutic applications of nanostructured zirconia in dentistry. RSC Adv. 2022;12:12773–12793. Available from: https://doi.org/10.1039/d2ra00006g

[54]. Quinn GD, Bradt RC. On the principles of fracture toughness measurement in brittle materials. J Am Ceram Soc. 2007;90(3):673–80. Available from: https://doi.org/10.1111/j.1551-2916.2006.01482.x

[55]. Gupta TK, Lange FF, Bechtold JH. Effect of stress-induced phase transformation on the strength of tetragonal zirconia alloys. J Mater Sci. 1978;13:1464–70. Available from: https://doi.org/10.1007/BF00553271

[56]. Chevalier J, Gremillard L, Deville S. Low-temperature degradation of zirconia and implications for biomedical implants. Annu Rev Mater Res. 2007;37:1–32. Available from: https://doi.org/10.1146/annurev.matsci.37.052506.08425

[57]. Munz D, Fett T. Ceramics: mechanical properties, failure behaviour, materials selection. Berlin: Springer; 1999. Available from: https://doi.org/10.1007/978-3-662-03841-1

[58]. Pradhan D, Wren AW, Misture ST, Mellott NP. Investigating the structure and biocompatibility of niobium and titanium oxides as coatings for orthopedic metallic implants. Mater Sci Eng C. 2016;58:918-26. Available from: http://dx.doi.org/10.1016/j.msec.2015.09.059

[59]. Santos C, Teixeira LHP, Daguano JKMF, Rogero SO, Strecker K, Elias CN. Mechanical properties and cytotoxicity of 3Y-TZP bioceramics reinforced with Al_2O_3 particles. Ceram Int. 2009;35:709-18. Available from: https://doi.org/10.1016/j.ceramint.2008.02.004

[60]. Sharanraj V, Ramesha CM, Kavya K, Vasantha Kumar, Sadashiva M, Chandan BR, Naveen Kumar M. Zirconia: as a biocompatible biomaterial used in dental implants. Adv Appl Ceram. 2021;120:63-8. Available from: https://doi.org/10.1080/17436753.2020.1865094

[61]. Akarsu MK, Basar AO, Sasmazel HT, Park J, Ozturk A. In vitro evaluation of tooth-colored yttria stabilized zirconia ceramics. J Asian Ceram Soc. 2021;9:1457-65. Available from: https://doi.org/10.1080/21870764.2021.1955491

[62]. Shin H, Ko H, Kim M. Cytotoxicity and biocompatibility of zirconia (Y-TZP) posts with various dental cements. Restor Dent Endod. 2016;41:167-75. Available from: http://dx.doi.org/10.5395/rde.2016.41.3.167

[63]. Keçeli SA, Alanyali H. A study on the evaluation of the cytotoxicity of Al_2O_3, Nb_2O_5, Ta_2O_5, TiO_2 and ZrO_2. Turk J Eng Environ Sci. 2004;28:49-54

[64]. Obata A, Hotta T, Wakita T, Ota Y, Kasuga T.
In vitro bioactivity and osteoblast cell response of niobium-releasing phosphate invert glasses. ACS Appl Mater Interfaces. 2012;4(11):5684–5690. Available from: https://doi.org/10.1021/am301614a

[65]. Dsouki NA, de Lima MP, Corazzini R, Gáscon TM, Azzalis LA, Junqueira VB, Feder D, Fonseca FLA. Cytotoxic, hematologic and histologic effects of niobium pentoxide in Swiss mice. J Mater Sci Mater Med. 2014;25(5):1301–1305. Available from: https://doi.org/10.1007/s10856-014-5153-0